CrystEngComm

PAPER

View Article Online
View Journal | View Issue

Cite this: *CrystEngComm*, 2014, **16**, 9245

Growth, structural and mechanical analysis of a single crystal of L-prolinium tartrate: a promising material for nonlinear optical applications

Kanika Thukral,[ab] N. Vijayan,*[b] Budhendra Singh,[c] Igor Bdikin,[c] D. Haranath,[b] K. K. Maurya,[b] J. Philip,[d] H. Soumya,[e] P. Sreekanth[f] and G. Bhagavannarayana[b]

Received 16th June 2014,
Accepted 23rd July 2014

DOI: 10.1039/c4ce01232a

www.rsc.org/crystengcomm

A single crystal of L-prolinium tartrate (LPT), which is an organic non linear optical material, was successfully synthesized and grown using a slow evaporation solution growth technique (SEST). The crystal structure and lattice parameters of the crystal were confirmed by powder X-ray diffraction and it was found that it belongs to the monoclinic crystal system with β = 100.380 and a noncentrosymmetric space group. The presence of strain in the grown ingot was calculated from powder X-ray diffraction measurements. The crystalline perfection was examined by high resolution X-ray diffractometry, which revealed that the crystal contained structural grain boundaries. The optical behavior of the grown specimen was analyzed by photoluminescence (PL) spectroscopy and its time resolved PL decay was calculated. The grown crystal adopted a step wise growth pattern with parallel striations, which was confirmed from the etching technique. Its ferroelectric and piezoelectric properties were also assessed. Its third order non linearity was assessed using an open aperture Z-scan technique. The thermal parameters of the LPT single crystal were calculated using a photopyroelectric technique. The mechanical strength of the single crystal at the micro level was observed by nanoindentation using the Oliver–Pharr method.

1. Introduction

In the past few decades it has been found that amino acid based compounds have potential nonlinear optical (NLO) behavior and show good mechanical strength. Nonlinear optical materials are proven to be suitable candidates for photonics and optoelectronic industries. These materials have been efficiently utilized for frequency conversion; optical switching and device fabrication which further depend on various properties of the material like transparency, birefringence, dielectric constant, refractive index and many more. Among organic and inorganic materials, the organic ones show excellent characteristics of NLO behavior due to weak van der Waals forces and hydrogen bonds with conjugated π electrons.[1–6] L-Prolinium tartrate is an organic NLO compound with an SHG efficiency of 95% of potassium dihydrogen phosphate (KDP) which is treated as the standard material for NLO measurements.[7] There are many reports available on organic materials like L-tartaric acid, L-alanine, L-arginine phosphate, L-prolinium picrate *etc.* that show higher orders of SHG.[8–11] In the present article, we report the crystalline perfection, strain calculations using the Hall–Williamson equation with the help of powder X-ray diffraction (PXRD), photopyroelectric (PPE) measurements and surface morphological studies of LPT. Nanoindentation studies were performed to find the load dependence and independence of hardness and to measure the Young's modulus using the Oliver–Pharr method. Various characterizations were performed for the grown compound that are explained in detail in the forthcoming sections.

2. Growth of a single crystal of L-prolinium tartrate

The slow evaporation solution growth technique (SEST) was adopted to grow a single crystal of L-prolinium tartrate ($C_5H_{10}NO_2^+ \cdot C_4H_5O_6^-$). The commercially available raw materials *i.e.* L-proline and L-tartaric acid were taken as received and their purity improved by repeated recrystallization processes. The purified salt was used in an equimolar ratio

[a] *Academy of Scientific and Innovative Research, CSIR- National Physical Laboratory, New Delhi-110 012, India*
[b] *CSIR-National Physical Laboratory, Crystal Growth and X-ray Analysis Section, Dr. K. S. Krishnan Road, New Delhi – 110 012, India. E-mail: nvijayan@nplindia.org, vjnphy@yahoo.com; Fax: +91 11 45609310; Tel: +91 11 45608263*
[c] *TEMA-NRD, Mechanical Engineering Department and Aveiro Institute of Nanotechnology (AIN), University of Aveiro, 3810–193 Aveiro, Portugal*
[d] *Department of Basic Sciences, Amal Jyothi College of Engineering, Kanjirappally, Kottayam 686518, Kerala, India*
[e] *Department of Instrumentation and STIC, Cochin University of Science and Technology, Cochin-682 022, India*
[f] *Light and Matter Physics Group, Raman Research Institute, Bangalore-560080, India*

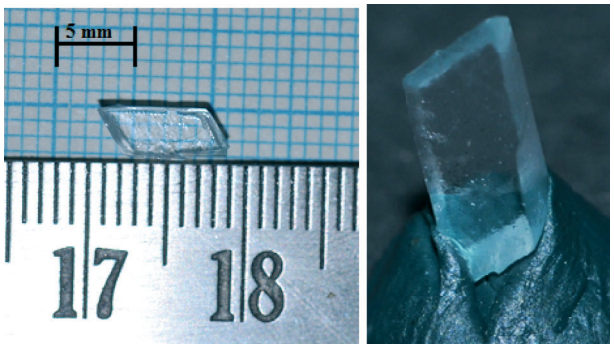

Fig. 1 Single crystal of L-prolinium tartrate with dimensions of $7 \times 4 \times 3$ mm^3.

and dissolved in double distilled water to make a saturated solution. This saturated solution was filtered using Whatmann filter paper. The purified solution was then placed in a constant temperature bath (CTB) at 34 °C. After the time span of 30 days a good quality crystal of dimensions $7 \times 4 \times 3$ mm^3 was harvested from the mother solution (shown in Fig. 1).

3. Characterization analyses

3.1. Powder X-Ray diffraction analysis (PXRD)

To determine the lattice parameters and space group of the crystal, powder X-Ray diffraction analysis was performed. The defect free single crystal was crushed into a fine powder and subjected to analysis by a Rigaku X-ray diffractometer with CuKα radiation (λ ~ 1.54 Å) and a scan speed of 4° min^{-1} over a range of 20°–70° and the recorded pattern is shown in Fig. 2a. Its lattice parameters, calculated using CheckCell software, were a = 5.0083 (Å), b = 17.6891 (Å), c = 6.5241 (Å), monoclinic system β = 100.381 with space group $P2_1$, all of which are in good agreement with the literature.[12–16] The strain in the lattice of the crystal was calculated using the Hall–Williamson equation $\beta \cos\theta = K\lambda/\tau + \eta \sin\theta$, where β, θ, K, λ and τ are the full width at half maximum (FWHM) of the diffraction peak, Bragg diffraction angle of the peak, Scherrer constant, wavelength of X-rays and crystallite size respectively. The plot is drawn between $\beta \cos\theta$ and $\sin\theta$, such that the slope of the curve gives the value of the strain (Fig. 2b). The value of the strain (η) is 0.0012 with a very slight error of 0.00146. This positive value suggests that the crystal contains some compressive strain which results in the interstitial defects in the crystal.[17]

3.2. Assessment of crystalline perfection

A PANalytical X'Pert PRO MRD high-resolution XRD system, with CuKα_1 radiation, was employed to assess the crystalline perfection of the crystal. The rocking curve of the crystal for the diffraction planes was recorded in symmetrical Bragg geometry using the natural facets by performing the ω scan[18] with a double-axis geometry. The monochromated X-ray beam incident on the specimen was obtained using a high-resolution four-bounce Ge (220) monochromator. The diffracted beam from the specimen was detected using a scintillation detector

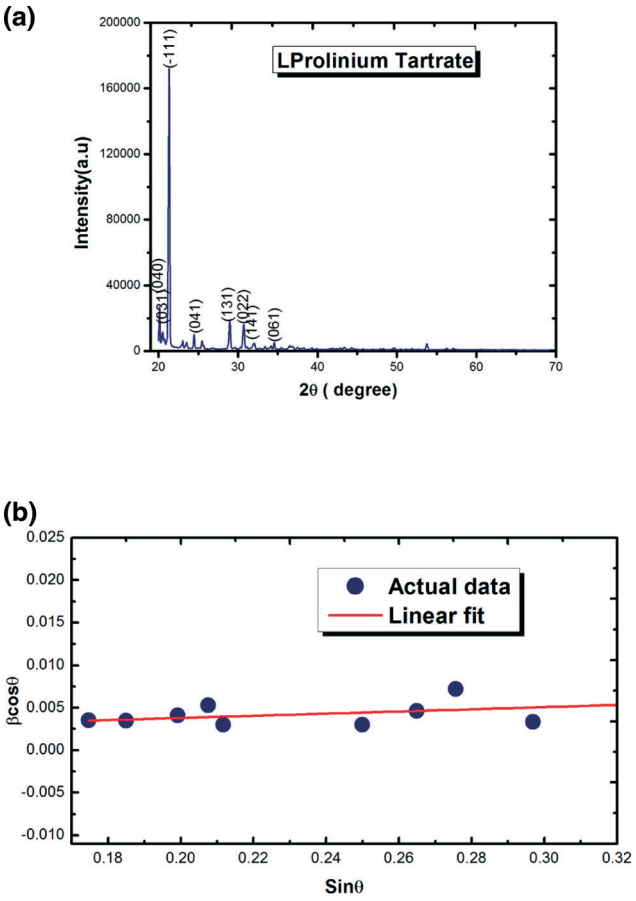

Fig. 2 (a) Powder X-Ray diffraction pattern of L-prolinium tartrate. (b) Strain calculation of L-prolinium tartrate.

without using any analyzer at the receiving stage (*i.e.* before the detector) to get all of the possible information like the individual peaks from structural grain boundaries, scattered intensity from the dislocations and other defects from the specimen crystal.

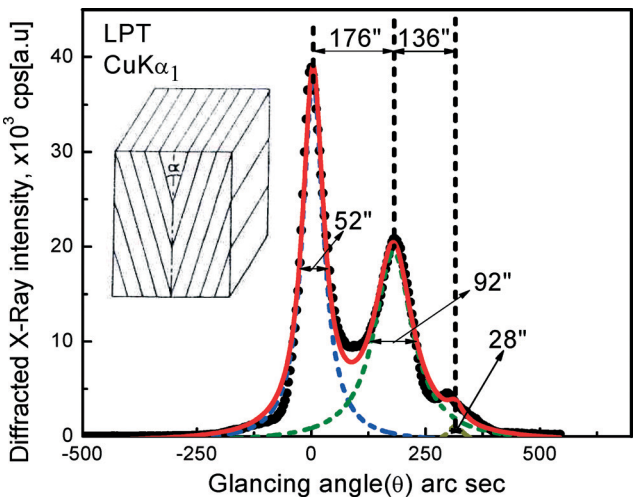

Fig. 3 Diffraction curve recorded for a typical LPT single crystal for (040) diffracting planes. Inset shows the schematic of a structural grain boundary.

Fig. 3 shows the high-resolution X-ray diffraction curve (DC) recorded for a typical specimen crystal (LPT) using (040) diffracting planes in symmetrical Bragg geometry by employing the MRD X-ray diffractometer described above with CuKα_1 radiation. As seen in the figure, the curve does not have only a single diffraction peak. The solid line, which fits well with the experimental points (filled circles), is the convoluted curve of three peaks using the Lorentzian fit. These multiple peaks depict the structural grain boundaries. According to our earlier convention,[19] depending on the tilt angle *i.e.* the misorientation angle (α) of the boundary with respect to the two adjacent crystalline regions on both sides of the boundary, the structural boundaries may be named as grain boundaries when $\alpha \geq 1$ deg, sub-grain or low angle boundaries when $\alpha > 1$ arc min but less than a deg and very low angle boundaries when $\alpha \leq 1$ arc min. The tilt angles of the observed structural grain boundaries are 176 and 136 arc sec, equivalent to 2.93 and 2.27 arc min respectively from their adjoining regions and hence all of the observed boundaries fall under the category of low angle boundaries. The FWHM (full width at half maximum) of the peaks corresponding to the observed boundaries are 52, 92 and 28 arc sec. It shows that the crystalline perfection is better than a previously reported example.[20] The relatively higher values of FWHM of the grains in comparison with those of the good crystals with only a few arc sec (ref. 21) indicate that impurities or solvent molecules[22] entrapped during the growth process could be responsible for the formation of these grain boundaries, where these may be segregated due to self-generated strains.[23] It may be mentioned here that such low angle boundaries could be detected with well-resolved peaks in the diffraction curve only because of the high-resolution of the diffractometer with a four bounce monochromator. Such defects may not have much influence on the NLO properties. However, a quantitative analysis of such unavoidable defects is of great importance, particularly in the case of phase matching applications as described in our recent article.[24]

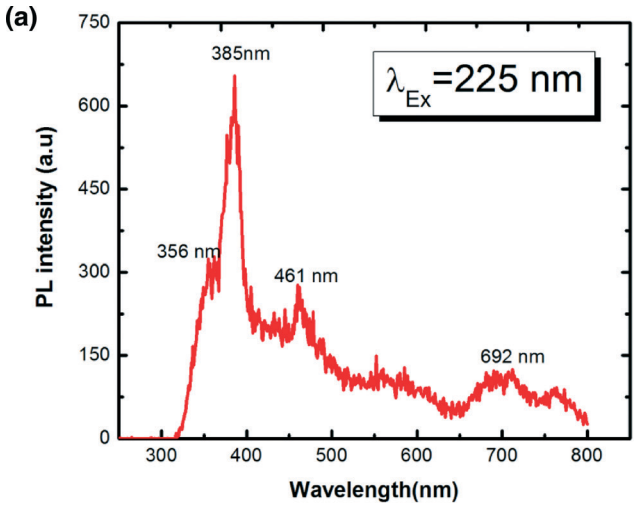

Fig. 4 (a) PL spectrum for a single crystal of L-prolinium tartrate; (b) time resolved PL decay and residual recorded at room temperature.

3.3. Time-resolved photoluminescence (PL)

Photoluminescence (PL) is another technique used to find out about the concentration of defects/imperfections present in a crystal by exciting a sample and recording its emission spectrum. Apart from PL, information about the decay kinetics of a material is highly important for the fabrication of laser devices from a crystal. The time-resolved PL (TRPL) decay curve indicates the life time of the exciton, which means the efficiency of radiative recombination after excitation is ceased. By calculating the decay time one is able to obtain the defect concentration as well. The PL and TRPL behavior of the title compound were recorded on an Edinburgh luminescence spectrometer (Model: F900) equipped with a microsecond xenon flash lamp as the source of excitation operating at ambient conditions. The PL spectrum is shown in Fig. 4a, which was recorded to the corresponding excitation wavelength of 225 nm. The peak maximum was observed at 385 nm, which is near to the visible region in accordance with the electromagnetic spectrum. The remaining peaks located at 461 and 692 nm were assigned to the defects present inside the crystal that were further confirmed by HRXRD. Usually, the TRPL decay curve is a multiexponential process with a series of long and short decay components but in the current situation it is observed to be biexponential. The actual behavior of TRPL decay curves can be expressed as

$$y = A + B_1 e^{-t/\tau_1} + B_2 e^{-t/\tau_1} \quad (1)$$

where τ_1 and τ_2 represent the fast and slow decay components of lifetime, and A, B_1 and B_2 are constants which determine the contributions of the fast and slow decay components.[25]

The decay profile of L-prolinium tartrate recorded in the range of 0–60 μs is shown in Fig. 4b. The curve obtained from the PL decay plot was exponential fitted and it shows a biexponential nature. The values of the decay constants are 1.0056 μs with 88% decay and 11.6 μs with 12% decay for the fast (τ_1) and slow (τ_2) decay components, respectively. This shows that 88% of the atoms in the material have a faster decay. The values of coefficients A, B_1, B_2 are −0.901, 2244.768, and 27.062 respectively. The residuals shown in Fig. 4b (inset) indicate the extent of best fitting performed on the actual decay curve.

3.4. Ferroelectric and piezoelectric measurements

The ferroelectric behavior of the sample was assessed using a ferroelectric loop tracer (make: Marine India). A defect free single crystal was taken for analysis and then coated with silver paste on both sides, which acted as an electrode. The area of the sample was 28 mm^2 and the thickness of the sample was 3 mm. Then the sample was placed in the holder and an electric field applied. The graph was then plotted between polarization and electric field as shown in Fig. 5. From the plot it is clear that the material is suitable for use in a lossy capacitor.

Piezoelectric measurements were carried out on a single crystal of L-prolinium tartrate using a PM-200 piezometer system with a frequency of 110 Hz and a dynamic force of 0.25 N at ambient conditions. The (040) surface of the sample was polished and then coated with silver paste for d_{33} analysis. The thickness of the crystal was 3.1 mm which was placed between the electrodes to make proper electrical contact. The force was gently applied to the sample and the observed value of piezoelectric constant was 4.4 pc N^{-1}.

3.5. Surface morphological studies

Etching is a revolutionary technique that reveals the crystal defects and growth mechanism. The etching technique provides information on the density and distribution of defects on the surface of a crystal which is helpful in assessing the surface quality of the crystal. In the present study doubly distilled water was used as the etchant for etching the (040) plane of the LPT crystal. The single crystal was dipped into doubly distilled water for 5 to 10 minutes for dissolution in order to ensure that the growth pattern, defects, hillocks, morphology *etc.* were more visible. Fig. 6a shows the surface of the crystal before etching which is completely smooth without any roughness visible. After 5–10 minutes Fig. 6b and c

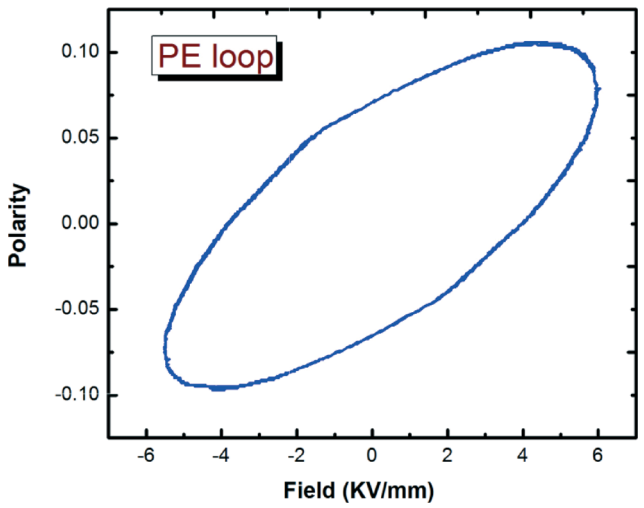

Fig. 5 PE loop for L-prolinium tartrate.

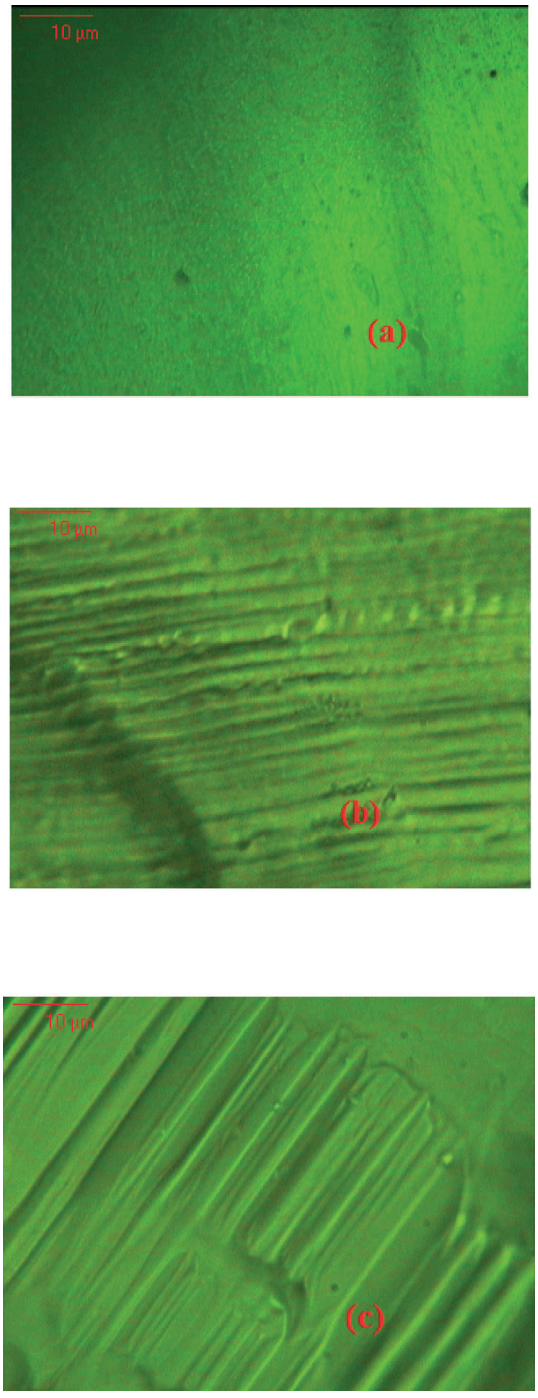

Fig. 6 Micrographs of the surface of (a) the as grown LPT crystal; (b) after 5 minutes of etching; (c) after 10 minutes of etching.

suggest that it has a step wise growth pattern. Such parallel striations shown in Fig. 6b and c are due to the high growth rate and two dimensional nucleation mechanism which occur when the solution becomes supersaturated.[26,27] It also confirms, with regards to the structure, that the semi-tartrate ions form hydrogen bonded strings and these strings are further connected to proline ions by forming a parallel layered network.[12]

3.6. Measurement of thermal transport parameters

The photopyroelectric (PPE) technique is a convenient non-destructive technique used to measure thermal properties, such as the thermal conductivity and specific heat capacity of solids, including small single crystals. The PPE technique is essentially a photothermal one in which the sample is irradiated by an intensity modulated beam of light (usually a laser), which generates thermal waves in the medium due to optical absorption which propagates through the medium. The corresponding periodic temperature rise on the opposite side of the sample is detected by a sensitive pyroelectric detector. The detector is usually supported by a backing medium. The sample thickness and modulation frequencies are selected so that the sample is thermally thick during the measurements. This ensures good thermal exchange between the sample and detector so that the detected signal is free of fluctuations.

The detected PPE signals are amplified and processed with a lock-in-amplifier. Measurement of the PPE signal amplitude and phase as a function of modulation frequency of the incident radiation enables one to determine the thermal effusivity and diffusivity of the sample, from which its thermal conductivity and specific heat capacity are determined.[28] In the present experiments we used a 120 mW He–Cd laser (λ = 442 nm) as the optical heating source and a 28 μm thick Ni–Cr coated PVDF film as the pyroelectric detector. The PPE signal amplitude and phase plotted against modulation frequency for the LPT crystal are shown in Fig. 7. The thermal diffusivity and effusivity determined from these plots as well as the thermal conductivity and specific heat capacity are tabulated in Table 1.

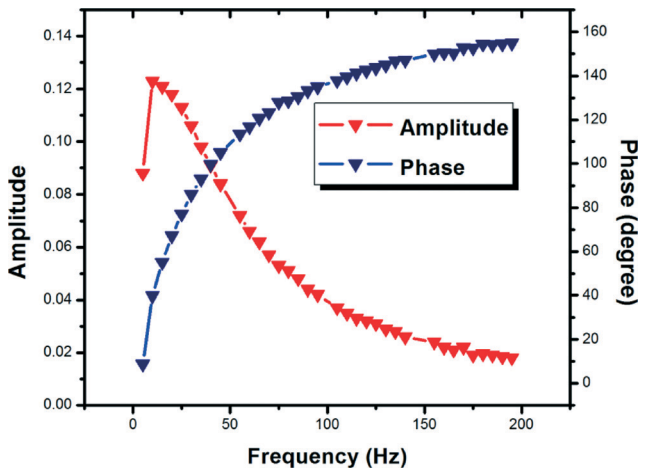

Fig. 7 PPE amplitude *vs.* frequency curve along with phase *vs.* frequency curve for a single crystal of LPT.

3.7. Third order non linearity studies

To investigate the non linear optical properties we employed the open aperture Z-scan technique[29] using the second harmonic output of a Q-switched Nd:YAG laser (Minilite continuum, 532 nm, 5 ns (FWHM)). The Gaussian beam was focused through a plano- convex lens of focal length 10.75 and the focal point is taken as $Z = 0$, since the beam is propagating in the Z-direction. At the focus point the density of energy is at its maximum and on either side it decreases. Therefore, the light fluence can easily be varied just by translating the sample stage along the z-axis. The sample was dissolved in distilled water and placed in a 1 mm cuvette. The cuvette was mounted on a stepper motor controlled translational stage and translated along the axis through the focus. The sample faces a different fluence at each position due to translation and the corresponding transmission is measured using a pyroelectric detector (laser probe Rj 7620) placed after the sample.[30] From the data obtained the nonlinear absorption coefficient could be calculated. Fig. 8 shows the open aperture Z-scans (inset) and the corresponding fluence dependent nonlinear transmissions obtained for L-prolinium tartrate at input laser pulse energies of 150 and 230 μJ. In general, the optical limiting behaviour of a medium can have contributions from effects such ESA (including excited singlet or triplet absorption, free-carrier absorption *etc.*), two- or three-photon absorption (2PA, 3PA), self-focusing/defocusing, thermal blooming, and nonlinear scattering. The two photon absorption coefficient can be calculated by numerically fitting the observed data using nonlinear transmission equations. Here the best fit is obtained for a process involving a two photon absorption (2PA) along with saturable absorption (SA). The obtained nonlinear parameters are presented in Table 2. The intensity dependent effective nonlinear absorption coefficient $\alpha(I)$ is given by

$$\alpha(I) = \frac{\alpha_0}{1+(I/I_s)} + \beta I \qquad (2)$$

where α_0 is the linear absorption coefficient at the wavelength of excitation, I is the input laser intensity, I_s is the saturation intensity, and β is the effective 2PA coefficient. For a given input intensity, the transmitted intensity is calculated by numerically solving the following propagation equation

$$\frac{dI}{dz'} = \left[\frac{\alpha_0}{1+(I/I_s)} + \beta I\right] I \qquad (3)$$

where z' is the propagation distance within the sample. The value of β numerically obtained from the fits indicates that the nonlinear absorption in the present case is arising from an effective two photon absorption, originating from a sequential excited state absorption involving real intermediate states. In the case of a genuine TPA, where the

Table 1 Thermal parameters of a single crystal of LPT

Sample	Thermal diffusivity, α ($\times 10^{-7}$ m^2 s^{-1})	Thermal effusivity, e (W m^{-2} K^{-1} s$^{+1/2}$)	Specific heat capacity, Cp (J kg^{-1} K)	Thermal conductivity, K (W mK^{-1})
L-Prolinium tartrate	9.16 ± 0.45	532 ± 8	469 ± 7	0.51 ± 0.01

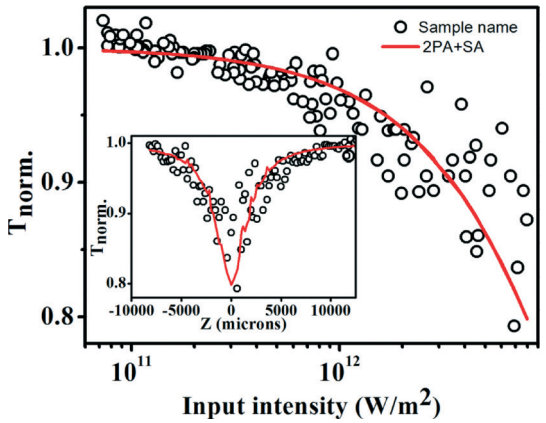

Fig. 8 Fluence dependent nonlinear transmission curve of L-prolinium tartrate, for an input laser pulse energy of 150 μJ. The open aperture Z-scan curve is shown in the inset.

transition states involved are virtual, the TPA coefficient is a constant, which is independent of incident laser fluence which is a very weak process. But a strong excited state absorption during an effective TPA depletes the ground state population significantly, so that the absorption coefficient is no longer a constant. It is clear from the Z-scan curves that the optical transmittance falls as input intensity increases, indicating the optical limiting behavior of the present sample. For an optical limiter the depth of the valley is a direct measure of the extent of optical limiting. The optical limiting material can be used as an optical sensor, also for protecting the human eye. The optical limiter should have a low limiting threshold, high optical damage threshold and fast response time with stability.

3.8. Mechanical strength analysis of LPT at the nanoscale

There is a constant interest in assessing the mechanical properties of crystals as they are closely related to their other physical and electrical properties,[31,32] and determine their performance when used in various device applications. For this, a hard indenter of a specific geometry is allowed to press the surface and based on the deformation beneath and around the indentation area (confined to a small volume) various parameters relating to the mechanical behaviour of the materials are evaluated. Nanoindentation is a technique used to evaluate the hardness of a material at the nanoscale. This technique is quite helpful for evaluating and understanding the mechanical behavior of a material in relation to its structure and/or bond strengths. In addition, surface texture, which is an important issue when the main interest is to understand the nature of the surfaces of a material, plays an important role in the functional performance of many engineering components. Taking advantage of high resolution atomic force microscopy (AFM), which allows precise topography imaging in a controlled way, we can visualize the surface and analyze the deformation beneath the indentation area.

The nanoindentation analyses were performed using a sharp Berkovich tip with a nominal edge radius of ~20 nm attached to a fully calibrated nanoindenter (TTX-NHT, CSM instruments). The indentation impressions were captured after unloading using atomic force microscopy (AFM). The experiments were performed such that the indentation axis was aligned normal to the (010) plane with different loads ranging from 5 to 150 mN. The approach speed, dwelling time and load/unload speed were kept at 2000 nm min^{-1}, 10 s and 20 mN min^{-1}, respectively. In a typical procedure 9 indentations at different locations on the specimen with different loads were made along the (010) direction. During each indentation run, a fully interfaced personal computer collected and stored data for the load and displacement as the indenter was driven into the sample (loading segment) and then withdrawn from it (unloading segment). The obtained results were analyzed and interpreted using the standard Oliver and Pharr method.[33] The hardness was calculated using the relationship

$$H = \frac{P_{\max}}{A_p} \quad (4)$$

where $P_{\max}$ is the maximum load applied by the indenter, and A_p is the projected contact area of indentation. For the present study, a proper calibration was made as per the standard procedure[34] given with the machine manual on a reference steel sample (provided with the system) with a known hardness using a 6 order polynomial area function given as[33]

Table 2 Nonlinear optical parameters calculated from the open aperture Z-scan measurements

Sample name	Input pulse energy (μJ)	Linear transmission (%)	β ($\times 10^{-11}$ m W^{-1})	I_s ($\times 10^{12}$ W m^{-2})	Optical limiting threshold ($\times 10^{13}$ W m^{-2})
L-Prolinium tartrate	150	75	0.6	40	5.201
	230	75	2.7	60	

$$A_p = 24.5h^2 + a_1h_c - a_2h^{1/2} + a_3h^{1/4} - a_4h^{1/8} + a_5h^{1/16}. \quad (5)$$

Furthermore, we know that indentation size, d, which is proportional to the value of the contact depth, h_c is also related to the peak load by

$$P = a_0 + a_1h_c + a_2h_c^2 \quad (6)$$

where a_0, a_1 and a_2 are constants. Furthermore, the parameter a_2, which is considered a measure of the load-independent hardness (H_o), and is related to the empirical formula

$$H_0 = ka_2 \quad (7)$$

(where k is a constant which depends on the indenter geometry, for the Berkovich indenter, the value of k is 1/24.5) was used for calculating the load independent hardness in the present case. The stiffness S (dP/dh), was determined using the initial slope of the unloading curve, which can be expressed as

$$h_c = h_{max} - \varepsilon \times \frac{P_{max}}{S} \quad (8)$$

where ε is the indenter constant and is equal to 0.75 and h_{max} is the maximum displacement of the indenter in the crystal when a load is applied. Different curves of loading and unloading with respect to the displacement were obtained using the relationship[35]

$$P = \alpha(h - h_f)^m \quad (9)$$

where P is the indentation load on the crystal, h is the displacement, h_f is the final displacement after completing the cycle of loading and unloading and α and m are empirical parameters. After getting the value of the load the slope value is calculated by differentiating the value of P

$$\left(\frac{dP}{dh}\right)_{h=h_{max}} = S = \alpha m(h_{max} - h_f)^{m-1}. \quad (10)$$

For the present case, a well polished surface was scanned using AFM in contact mode for obtaining the roughness parameters for the surface under nanoindentaion. A nearly very smooth (Fig. 9a) surface was obtained with various scratch lines due to polishing seen on the surface with typical depths in the order of a few 100 nm. Fig. 9b shows the roughness profile of the single crystal of LPT along the (010) plane. The calculated RMS roughness parameter in the order or 72 nm was obtained. Fig. 10a shows representative P–h curves obtained on the (010) facets of the single crystals of L-prolinium tartrate using a Berkovich tip. A smooth loading part was observed indicating a plastic deformation, which occurs underneath the indenter so as to accommodate the strain imposed by the sharp indenter. In addition, a relatively homogeneous loading curve with no traces of any 'pop-in' features (*i.e.* discrete displacement bursts) except for a few serrations was observed. However, a pile-up was evident from the crystal after indentation (typical imprint made by 50 mN force) as shown in the insets of Fig. 10. Fig. 10b shows the cross section profile for the depth after indentation with a 50 mN load. A good correlation between the nanoindentation depth profile and the profile from the AFM were seen (Fig. 10a and b). The obtained P–h curves were analyzed using eqn (4–10) for obtaining various parameters associated with the mechanical behavior of the single crystal of L-prolinium tartrate, which are listed in Table 3. A decrease in the value of hardness with increasing load was observed, suggesting a load dependent hardness parameter. Fig. 11 shows the variation of the contact depth with peak load. The contact depth was found to increase as the peak load increased, due to a load dependant hardness, suggesting that the indentation size can have an effect on the hardness of the material, which is proportional to the values of contact depth and peak load. For calculating the load independent hardness parameter using eqn (6), the variation of contact

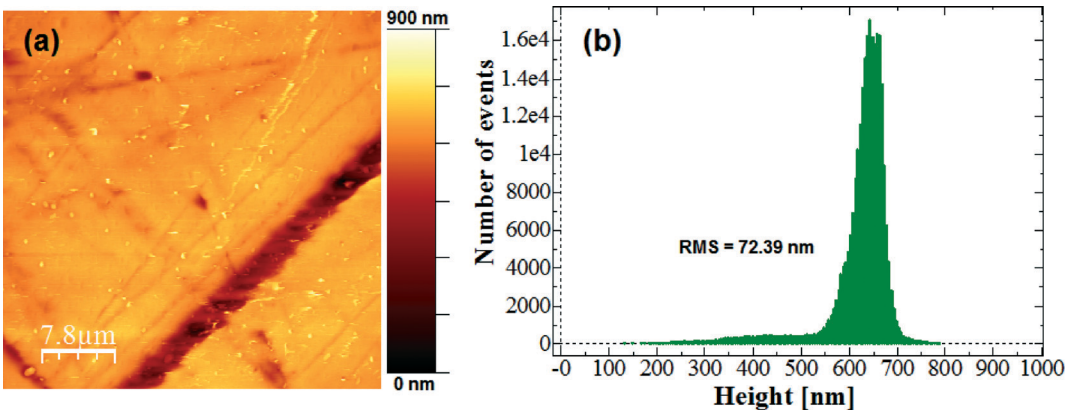

Fig. 9 (a) AFM topography image of the LPT crystal after polishing along the (010) plane and (b) roughness profile of the AFM image.

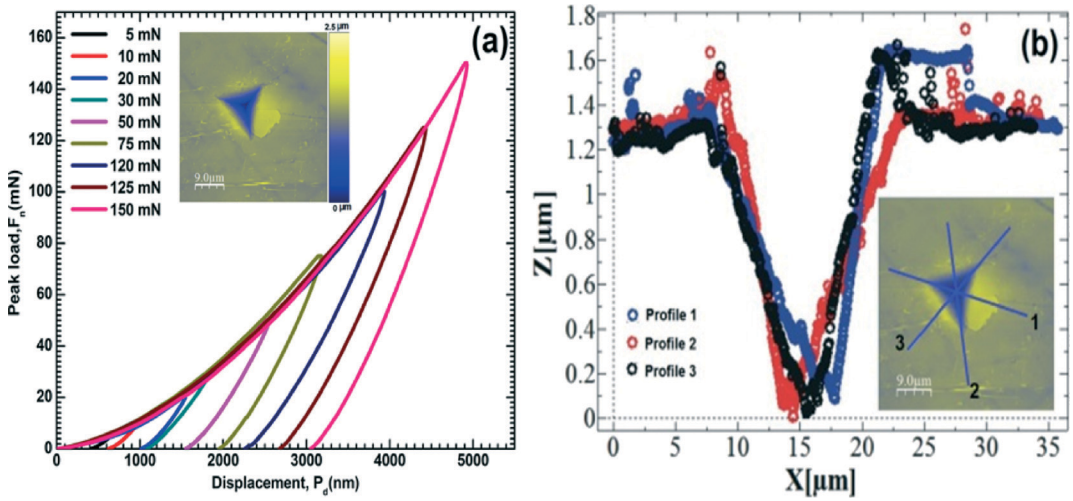

Fig. 10 (a) Load–displacement curves of a single crystal of L-prolinium tartrate along the (010) plane and (b) depth profile of the indentation imprint after applying a 50 mN load. The insets of figures show a typical imprint made after indentation along the (010) plane.

Table 3 Various obtained parameters associated with the mechanical properties of a single crystal of LPT along the (010) plane

F (mN)	H_{IT} (GPa)	E_{IT} (GPa)	h_m (nm)	S [mN nm^{-1}]	h_c (nm)	h_r (nm)	h_p (nm)	m
10	654.34	7.96	982.81	0.04	790.18	729.76	624.45	1.38
20	507.03	6.84	1545.42	0.055	1268.26	1179.86	1021.72	1.41
30	619.93	5.86	1851.32	0.052	1404.91	1273.77	1092.03	1.30
50	509.33	5.49	2551.88	0.069	2000.48	1830.50	1568.31	1.36
75	492.65	5.30	3178.02	0.084	2490.45	2279.34	1975.26	1.35
100	452.34	4.31	3935.97	0.082	3001.17	2714.67	2300.70	1.35
125	429.84	4.42	4436.03	0.096	3441.60	3136.00	2705.87	1.35
150	402.08	4.49	4929.99	0.111	3897.89	3575.41	3085.47	1.38

depth with peak load was plotted (Fig. 11) and fitted with the polynomial function for obtaining the constants a_0, a_1 and a_2. The value of a_2 for the present case was obtained as 3.224×10^{-6} mN nm^{-2}. Furthermore, using eqn (7), the value of the load independent hardness (H_o) was calculated to be 131 MPa. Fig. 12 shows the variation of the Young's modulus extracted from the analysis of the load–displacement curves as a function of peak load. A significant decrease in the Young's modulus was observed with increasing peak load. This dependence is attributed to the indenter tip rounding. It is to be noted that the tip imperfection of the indenter does not affect the hardness results.[36] In a recent study, Antunes *et al.* concluded that a correction of the geometry of the

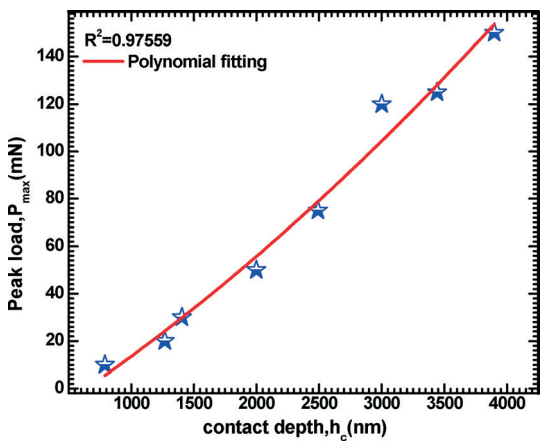

Fig. 11 Variation of contact depth with peak load.

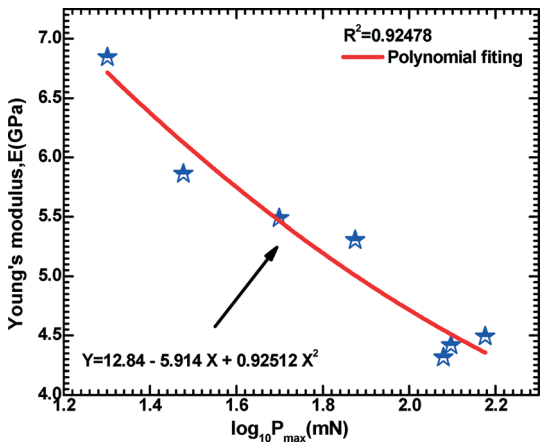

Fig. 12 Variation of Young's modulus extracted from the analysis of the load–displacement curves as a function of peak load along the (010) plane.

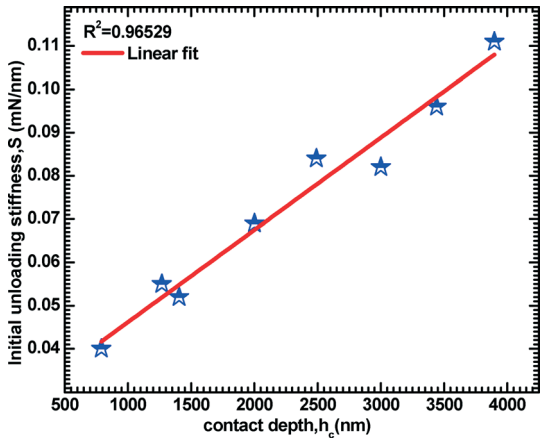

Fig. 13 Variation of initial loading stiffness, *S*, with the contact depth at peak load.

Vickers indenters with offset, using the respective area function, is enough to obtain accurate values of the mechanical properties, namely the Young's modulus and the hardness.[37] However for understanding the degree of tip rounding, the variation of initial loading stiffness, *S*, with the contact depth at peak load, h_c for the (010) plane was plotted (Fig. 13). The relationship of *S* with h_c is given as

$$S = a + bh_c \quad (11)$$

where *a* is a constant related to indentation tip rounding and the slope *b* is related to the reduced Young's modulus. A linear relationship between the initial unloading stiffness, *S* and the contact depth at peak load was observed. The reduced Young's modulus was extracted from the slope of the linear fitted curve. The constant '*a*' and the slope for the (010) plane were found to be 0.0241 and 2.1332×10^{-5} mN nm^{-2}, respectively. The reduced Young's modulus was estimated from the slope and found to be 21 GPa for the indentation made on the (010) plane. However, no data in the literature are available for direct comparison of the obtained values. Furthermore, the best fit curve should pass through the origin, however, a significantly larger value of the intercept, ('*a*') 0.0241, was observed due to indenter tip rounding.

4. Conclusion

In the present report, a good quality single crystal was grown by the slow evaporation solution growth technique. The grown crystal was subjected to powder XRD for primary identification of its lattice parameters and its strain was also calculated. The crystalline perfection was assessed by high resolution X-ray diffraction and found to be reasonably good. Its optical properties were analyzed by photoluminescence. The presence of defects on the surface was examined by etching studies using distilled water as an etchant. Furthermore its third order non linearity, thermal properties, PE loop and piezoelectric coefficient were determined. The load dependent and independent hardness along the Young's modulus was calculated by nanoindentation.

Acknowledgements

The authors are highly thankful to Dr. R.C. Budhani, Director, NPL for his constant support and encouragement. One of the authors (K.T.) is thankful to the U.G.C (University of Grant Commission) for providing the research fellowship. Budhendra Singh would like to express their personal thanks to FCT (Fundaçãopara a Ciência e a Tecnologia) for post-doctoral research grants with reference numbers SFRH/BPD/76184/2011.

References

1 H. S. Nagaraja, V. Upadhyaya, P. Mohan Rao, P. Sreeramana Aithal and A. P. Bhatt, *J. Cryst. Growth*, 1998, **193**, 674–678.
2 M. R. Suresh Kumar, H. J. Ravindra, A. Jayarama and S. M. Dharmaprakash, *J. Cryst. Growth*, 2006, **286**, 451–456.
3 P. Srinivasan, M. Gunasekaran, T. Kanagansekaran, R. Gopalakrishnan and P. Ramasamy, *J. Cryst. Growth*, 2006, **289**, 639–646.
4 N. Vijayan, G. Bhagavannarayana, R. Ramesh Babu, R. Gopalakrishnan, K. K. Maurya and P. Ramasamy, *Cryst. Growth Des.*, 2006, **6**, 1542–1546.
5 S. Suresh, A. Ramanand, D. Jayaraman and P. Mani, *Rev. Adv. Mater. Sci.*, 2012, **30**, 175–183.
6 D. Xu, M. Jiang and Z. Tan, *Acta Chim. Sin.*, 1983, **41**, 570–573.
7 K. Moovendaran, V. Jayaramakrishnan and S. Natarajan, *Photonics Optoelectron.*, 2014, **3**, 9–14.
8 S. A. Martin Britto Dhas, M. Suresh, G. Bhagavannarayana and S. Natarajan, *J. Cryst. Growth*, 2007, **309**, 48–52.
9 T. Raghavalu, G. Ramesh Kumar, S. Gokul Raj, V. Mathivanan and R. Mohan, *J. Cryst. Growth*, 2007, **307**, 112–115.
10 A. M. Petrosyan, R. P. Sukiasyan, H. A. Karapetyan, S. S. Terzyan and R. S. Feigelson, *J. Cryst. Growth*, 2000, **213**, 103–111.
11 T. Uma Devi, N. Lawrence, R. Ramesh Babu and K. Ramamurthi, *J. Cryst. Growth*, 2008, **310**, 116–123.
12 M. Subha Nandhini, R. V. Krishnakumar and S. Natarajan, *Acta Crystallogr., Sect. C: Cryst. Struct. Commun.*, 2001, **57**, 423–424.
13 S. A. Martin and S. Natarajan, *Cryst. Res. Technol.*, 2007, **42**, 471–476.
14 S. Suresh, P. Mani and K. Anand, *Int. J. Comput. Appl.*, 2012, **43**, 35–40.
15 S. Suresh, A. Ramanand, D. Jayaraman and P. Mani, *J. Optoelectron. Adv. Mater.*, 2010, **4**, 1743–1746.
16 S. Tamilselvan, A. Cyrac Peter, C. K. Mahadevan, J. Madhavan and M. Vimalan, *Arch. Appl. Sci. Res.*, 2011, **3**, 180–185.
17 S. K. Kushwaha, K. K. Maurya, N. Vijayan, B. Kumar, R. Bhatt, S. Ganesamoorthy and G. Bhagvannarayana, *CrystEngComm*, 2012, **14**, 3297–3305.
18 G. Bhagavannarayana and S. K. Kushwaha, *J. Appl. Crystallogr.*, 2010, **43**, 154–162.

19 G. Bhagavannarayana, R. V. Ananthamurthy, G. C. Budakoti, B. Kumar and K. S. Bartwal, *J. Appl. Crystallogr.*, 2005, **38**, 768–771.
20 S. Natarajan, K. Moovendaran, J. Kalyana Sundar, G. Bhagavannarayana and S. A. Martin Britto Dhas, *J. Miner. Mater. Charact. Eng.*, 2011, **10**, 913–921.
21 P. V. Dhanaraj, C. K. Mahadevan, G. Bhagavannarayana, P. Ramasamy and N. P. Rajesh, *J. Cryst. Growth*, 2008, **310**, 5341–5346.
22 K. Senthilkumar, S. Moorthy Babu and G. Bhagavannarayana, *J. Appl. Crystallogr.*, 2011, **44**, 313–318.
23 G. Bhagavannarayana, P. Rajesh and P. Ramasamy, *J. Appl. Crystallogr.*, 2010, **43**, 1372–1376.
24 G. Bhagavannarayana, B. Riscob and M. Shakir, *Mater. Chem. Phys.*, 2011, **126**, 20–23.
25 N. Vijayan, J. Philip, D. Haranath, B. Rathi, G. Bhagavannarayana, S. K. Halder, N. Roy, M. S. Jayalakshmy and S. Verma, *Spectrochim. Acta, Part A*, 2014, **122**, 309–314.
26 R. H. Rao and S. Kalainathan, *Mater. Res. Bull.*, 2012, **47**, 987–992.
27 G. H. Sun, G. H. Zhang, X. Q. Wang and D. Xu, *J. Cryst. Growth*, 2011, **316**, 132–136.
28 C. P. Menon and J. Phillip, *Meas. Sci. Technol.*, 2000, **11**, 1744–1749.
29 M. Sheik-Bahae, A. A. Said, T. H. Wei, D. J. Hagan and E. W. V. Stryland, *IEEE J. Quantum Electron.*, 1990, **26**, 760–769.
30 Reji Philip, Panit Chantharasupawong, Huifeng Qian, Rongchao Jin and J. Thomas, *Nano Lett.*, 2012, **12**, 4661–4667.
31 S. K. Jat, N. Vijayan, A. Krishna, J. Philip, S. Verma, I. Bdikin, B. Singh, G. Bhagavannarayana and S. K. Halder, *CrystEngComm*, 2013, **15**, 10034–10042.
32 I. Bdikin, B. Singh, J. Suresh Kumar, M. P. F. Graça, A. M. Balbashov, J. Grácio and A. L. Kholkin, *Scr. Mater.*, 2013, **74**, 76–79.
33 W. C. Oliver and G. M. Pharr, *J. Mater. Res.*, 1992, **7**, 1564–1583.
34 A. C. Fischer-Cripps, *Surf. Coat. Technol.*, 2006, **200**, 4153–4165.
35 M. F. Doerner and W. D. Nix, *J. Mater. Res.*, 1986, **1**, 601–609.
36 N. A. Sakharova, J. V. Fernandes, J. M. Antunes and M. C. Oliveira, *Int. J. Solids Struct.*, 2009, **46**, 1095–1104.
37 J. M. Antunes, L. F. Menezes and J. V. Fernandes, *Int. J. Solids Struct.*, 2007, **44**, 2732–2747.

